Frustrated Rotator Crystals and Glasses of Brownian Pentagons

Kun Zhao[1,2] and Thomas G. Mason[1,2,3,*]

[1]Department of Physics and Astronomy, University of California–Los Angeles, Los Angeles, California 90095, USA
[2]Department of Chemistry and Biochemistry, and University of California–Los Angeles, Los Angeles, California 90095, USA
[3]California NanoSystems Institute, University of California–Los Angeles, Los Angeles, California 90095, USA

(Received 19 February 2009; published 10 November 2009)

Two-dimensional Brownian dispersions of microscale pentagonal platelets exhibit rich structural and dynamical behavior as the particle area fraction, ϕ_A, is increased. As ϕ_A is raised above 0.66, a rotator crystal forms, and while in an equilateral hexagonal lattice, pentagons still explore all angles as they rotationally diffuse. At larger ϕ_A, the interference of the tips of neighboring pentagons causes rotational dynamical heterogeneity; particle rotations become nonergodic, the hallmark of a frustrated rotator crystal. Upon further compression, the quenched-in rotational disorder and inability of pentagons to fully tile a flat plane creates spatial defects, precluding access to a dense striped crystalline packing.

DOI: 10.1103/PhysRevLett.103.208302 PACS numbers: 82.70.Dd, 64.60.−i, 68.65.−k, 81.30.−t

Colloids, such as biomolecules and nanoparticles, can behave in interesting ways when confined to two-dimensional surfaces and films. For example, the nature of melting in 2D is still actively debated and is quite different from that in 3D, where it is a first order transition [1–6]. The collective structure and dynamics of Brownian particles that diffuse in 2D can be strongly affected by their surface density and interactions. A full understanding of how the shapes of hard colloidal objects, confined to a 2D flat surface, can affect their collective structure and dynamics has remained elusive. Although the phase behavior of colloidal particles having different shapes has received some attention [7–13], no general framework has been developed for understanding the structural and dynamical properties of simple thermally excited ''hard'' Brownian objects, such as equilateral polygons, on a flat plane.

Pentagons represent the simplest equilateral polygon for which flat 2D space cannot be fully tiled. In particular, when the particle area fraction ϕ_A becomes high enough, the pentagonal shape interferes with full tiling (i.e., the limit $\phi_A = 1$). A nonequilateral hexagonal lattice, consisting of alternating stripes of pentagons that point head-to-tail in opposite directions, creates the highest known $\phi_A^{\mathrm{ASX}} = 0.921$ [14–16]. In experiments, this high-density alternating striped crystal (ASX) has been formed with macroscopic particles using nonthermal placement [15,17], but it is not clear that this structure could be observed in 2D Brownian systems of pentagons in which thermal fluctuations play an important role.

Recently, top-down particle production methods have provided a wide diversity of monodisperse colloidal shapes [18–23], opening up opportunities for exploring interesting scientific questions at the mesoscale. In particular, microscale pentagonal polymer platelets have been mass produced using optical lithographic methods [18] and dispersed in a viscous liquid. Such dispersions are ideal for optically studying interesting phase behavior and even individual and collective particle dynamics.

In this Letter, we present the observed dynamic and structural behavior of a model dispersion of Brownian pentagonal platelets (i.e., ''pentagons'') confined to a 2D plane, and focus on the rotational ergodic-nonergodic transition. Besides a disorder-order transition at low-density range ($\phi_A \leq 0.66$), we also observe dynamical heterogeneity and the onset of rotational jamming of pentagons as ϕ_A is further increased and the system transforms from a hexagonal rotator crystal (RX) phase to a frustrated rotator crystal (FRX) state. The rotational jamming of particles in 2D, while maintaining positional order, is likely to be a key feature for thermal dispersions of many different shapes, not just pentagons. At higher ϕ_A, a frustrated rotator glass (FRG) state is observed, where G refers to glassy positional disorder and FR refers to frustrated rotational dynamics.

Using photolithography, we make equilateral pentagons of a polymer (SU-8) [18] having dimensions: edge length $a \approx 1.8\ \mu$m, center-to-vertex distance $r_0 \approx 1.53\ \mu$m, center-to-edge distance $r_i \approx 1.24\ \mu$m, and thickness $L = 2.0 \pm 0.1\ \mu$m. The pentagons are stabilized against aggregation by adsorbed sodium dodecyl sulfate (SDS: 1 mM) to form an aqueous dispersion. A rectangular optical cuvette is filled with a dilute mixture of a pentagon dispersion and a dispersion of a depletion agent (see details in supplementary material (SM) [24]). Since the polymer's density $\rho_{\mathrm{SU8}} \approx 1.2\ \mathrm{g/cm^3}$ exceeds that of water, the pentagons sediment to the lower glass wall. The depletion agent causes anisotropic roughness-controlled depletion attractions [25], so the pentagons are forced to lie flat, parallel to the lower wall, yet still diffuse in the plane. Because the edges of the pentagons are significantly rougher than their faces, any residual attraction between the edges of two pentagons is less than k_BT, so ''hard'' short-range repulsions dominate in-plane particle interactions. This approach provides a 2D monolayer of platelets that do not exhibit Brownian tipping out of the plane and also do not experience capillary attractions that are typical of particles at fluid-fluid interfaces. The Debye length in the system is

$L_D \approx 4$ nm, much smaller than a and L. Pentagons are concentrated in 2D by tilting the cuvette about its long axis at angles between 1° and 6°, creating a slowly varying spatial gradient in ϕ_A. Specific ϕ_A are viewed microscopically along the length of the cuvette. A single field of view (74 μm × 55 μm) reveals about 500 particles at high ϕ_A. By adapting video particle tracking microscopy [26], we measure the center positions of the pentagons and also their rotational angles, $\theta(t)$, which are then used to calculate spatial and bond-orientational order parameters, $S(\phi_A)$ and $\psi_6(\phi_A)$, correlation functions [5,6,16] (see details in SM [24]), as well as rotational dynamics.

In Fig. 1, we show micrographs of configurations of dense thermal pentagons [insets—fast Fourier transforms (FFTs)]. When $\phi_A \leq 0.60$, an isotropic phase (I) is found [Fig. 1(b)]. As ϕ_A increases, both the translational and the bond-orientational order increase [Fig. 1(c)], and the FFT of the image shows six wider peaks. Because of the limited spatial extent of our observations, which are made at high magnification in order to track rotational dynamics of individual pentagons, we have some evidence suggesting but cannot conclusively identify a hexatic phase that has been predicted by KTHNY theory and reported for some experimental systems [1,4–6]. At yet higher ϕ_A, a RX phase forms [Fig. 1(d)], and very sharp peaks in FFT image indicate nearly perfect translational order. Above an effective "overlap" concentration, $\phi_A = 0.69$, corresponding to hexagonal packing of disks having radii r_0, tip-tip interactions between neighboring pentagons become important and significantly affect rotational dynamics. Because of this interference of the tips of the pentagons, the FFT peaks become somewhat wider, and the system of pentagons rotationally jams, even though it preserves translational quasi-long-range order (QLRO), yielding an FRX state [Fig. 1(e)]. (Jammed states can be path dependent and thus may reflect the history of osmotic compression in 2D. That is why we use the terminology FRX state and not FRX phase.) At higher $\phi_A = 0.88$ (tilt angle of 6°), the translational order can no longer be maintained due to the local geometric frustration introduced by strong interactions between neighboring pentagons, so the FRX state begins to disorder positionally and becomes an FRG state [Fig. 1(f)]. In the FRG state, local jamming causes defects, grain boundaries, and translational disorder; groups of pentagons form small crystallites having different lattice orientations, so the FFT displays a polycrystalline signature. Similar polycrystalline structure has also been found for shape-polydisperse polygons [13]. Because of packing frustration under compression, we do not observe an alternating striped crystalline (ASX) structure at high ϕ_A.

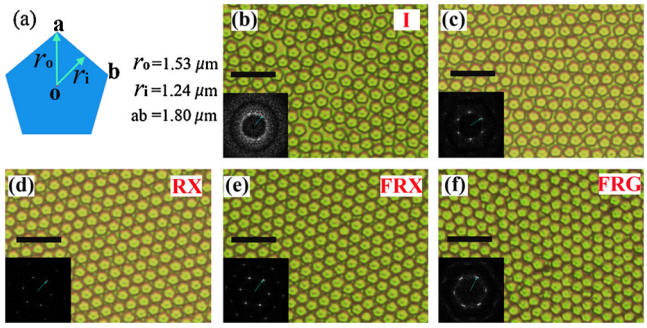

FIG. 1 (color online). (a) Face-on schematic view of a pentagonal platelet: r_0 is the outer radius of the circumscribed circle and r_i is the inner radius of the inscribed circle. (b)–(e) Optical microscope images of Brownian pentagons in 2D at area fractions ϕ_A: (b) 0.60, (c) 0.63, (d) 0.73, (e) 0.76, and (f) 0.88 (scale bars = 10 μm). Insets: fast Fourier transforms (FFTs) of the images.

As the system is compressed from I to RX phases (possibly through a hexatic phase), the spatial and bond-orientational order parameters both increase rapidly and are highly correlated [Fig. 2(a)]. As ϕ_A further increases, they do not change significantly even as rotational frustration becomes important. However, at even larger ϕ_A, the

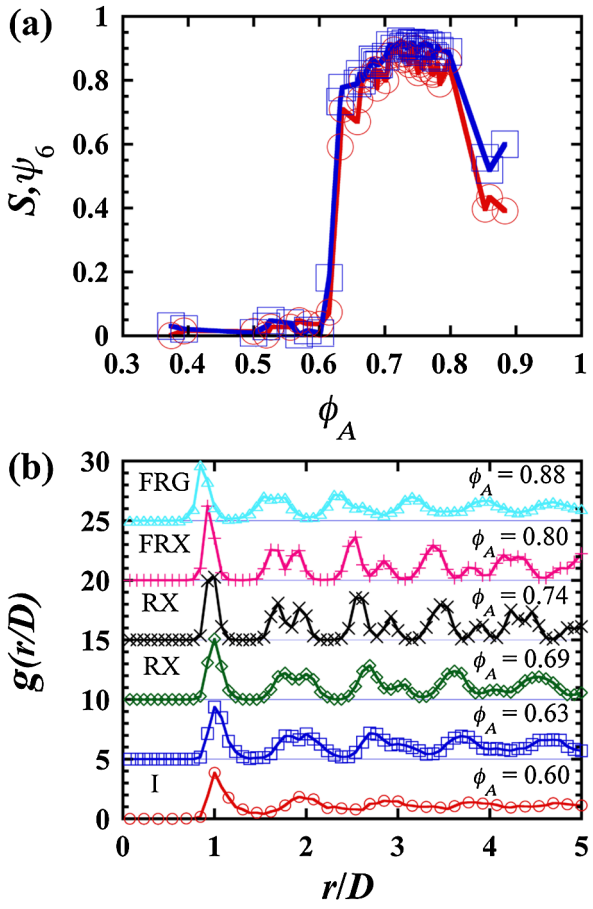

FIG. 2 (color online). Measures of spatial order and bond-orientational order and pair correlations as a function of area fraction ϕ_A. (a) Order parameters: spatial-S (red circles); sixfold-bond-orientational-ψ_6 (blue squares). (b) Pair correlation function $g(r/D)$ in order from bottom to top: $\phi_A = 0.60$ (○), 0.63 (□), 0.69 (◇), 0.74 (×), 0.80 (+), and 0.88 (△); results have been shifted up for clarity. The effective tip overlap spacing is: $D = 2r_0 \approx 3.1$ μm.

FRG state is marked by defects and positional disorder, and the onset of the translationally jammed glass is reflected by sharp drops in S and ψ_6.

We calculate the pair correlation function, $g(r)$, where r is the center-to-center separation between pairs of pentagons [Fig. 2(b)]. As ϕ_A increases, the second peak in $g(r)$, observed for I phase, splits into two peaks characteristic of an equilateral hexagonal crystal, and the first peak increases in height and narrows. Large hexagonal crystals can be observed over a large field of view in the RX phase, so coherent features in $g(r)$ extend to large r. As spatial disorder increases towards the largest ϕ_A we explore, the peaks weaken and become broader; the pair of second peaks become less distinguishable.

Since the RX-FRX transition cannot be captured by spatial order parameters and $g(r)$, we track the rotation of pentagons $\theta(t)$ at different ϕ_A, thereby revealing the onset of rotational dynamical heterogeneity and nonergodicity. Figure 3(a) shows sample rotational trajectories, $\theta(t)$, for individual pentagons in the RX phase, FRX state, and FRG state, and Fig. 3(b) displays the respective histograms $p(\theta)$. In the RX phase, pentagons can rotate to explore all angles, and interference of the tips of neighboring pentagons is infrequent, since $r > 2r_0$. Consequently, $p(\theta)$ in the RX phase is distributed over a wider range and lacks structure. However, as ϕ_A is increased, tips of neighboring pentagons begin to interfere more frequently, and locally cooperative translational and rotational fluctuations are needed to provide enough space for at least some tips to pass each other. Thus, near the onset of rotational jamming, θ fluctuates about a first value before tip exchange occurs, and then it fluctuates around a different second value, separated by an angle typically between $\pi/3$ and $2\pi/5$. Correspondingly, $p(\theta)$ exhibits multiple discrete peaks having average separation $\Delta\theta \approx 1.3$ rad. These are hallmarks of rotational dynamical heterogeneity in the approach to a rotational glass transition. As ϕ_A is further increased, the rotations are further confined; only a few tip-tip passages are infrequently observed. In the full FRX state, rotational tip-tip passage is no longer observed over very long time scales (e.g. days), and $p(\theta)$ shows only a single peak. Likewise, at higher ϕ_A in the FRG state, the rotational behavior remains nonergodic.

The rotational autocorrelation function $C_{\rm rot}(t) = \langle \vec{n}_i(\tau)\vec{n}_i(t+\tau)\rangle$, where $\vec{n}_i$ is the unit vector of orientation of pentagon i, and the mean square angular displacement $\langle \Delta\theta^2(t)\rangle$ further illustrate the rotational dynamic heterogeneity during the approach to the fully nonergodic rotator glass. Figure 4 shows the average $C_{\rm rot}(t)$ and $\langle \Delta\theta^2(t)\rangle$ (inset). Near the FRX state, $C_{\rm rot}(t)$ follows a nearly single exponential decay and $\langle \Delta\theta^2(t)\rangle$ approaches pure diffusion at longer times. As ϕ_A is increased, the decay of $C_{\rm rot}(t)$ can be fit by a stretched exponential, as has been found in structural glasses (see, e.g., [27]), the multiple relaxation time scales arise from dynamical heterogeneity resulting from tip-tip rotational hindrances. In the FRX and FRG states, particles do not rotate beyond a small range of angles, so $C_{\rm rot}(t)$ decays only a very small amount at early times, corresponding to highly confined rotational diffusion, and no tip-tip passage occurs. Moreover, as ϕ_A is increased, $\langle \Delta\theta^2(t)\rangle$ becomes subdiffusive over longer time scales, and, when the system reaches the full FRX state, $\langle \Delta\theta^2(t)\rangle$ exhibits a plateau over the measured temporal range, indicating the rotational jamming of particles and fully nonergodic behavior. Although there appears to be at least some degree of decoupling between positional ordering and rotational dynamics in the FRX state, as the system is further compressed into the FRG state, the quenched-in rotational disorder also contributes to positional disorder, precluding access to the ASX packing. Because of the strong translational and rotational jamming, once pentagons have been osmotically jammed into the FRG state, they remain disordered and are unable to nucleate a denser ASX structure even after several months.

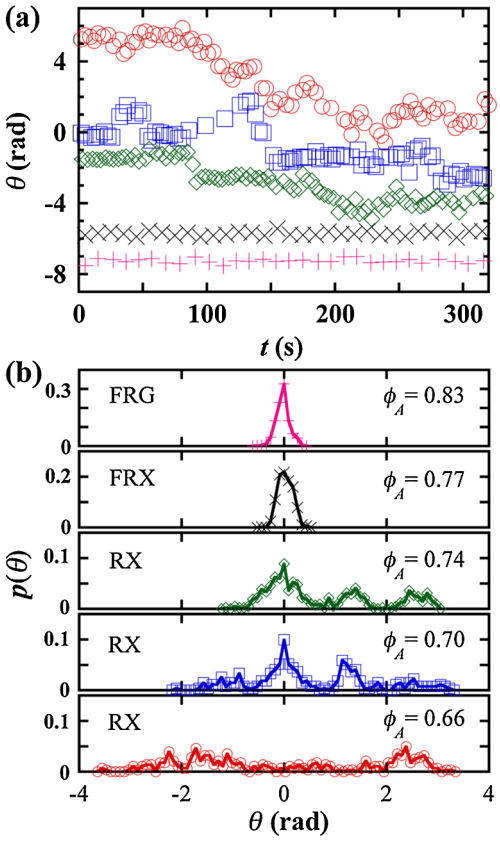

FIG. 3 (color online). Pentagon rotational dynamics at different particle area fractions ϕ_A: (a) Rotation angles θ as a function of time t. For clarity, $\theta(t)$ for each particle has been shifted by a constant angle. Symbols: $\phi_A = 0.66$ (○); 0.70 (□); 0.74 (◇); 0.77 (×); 0.83 (+). (b) Histograms of trajectories from part (a) showing probabilities p at a particular θ. Curves have been shifted by a constant angle to compare peak positions at different ϕ_A. Multiple peaks in $p(\theta)$, spaced at roughly $\Delta\theta \approx 1.3$ rad, indicate dynamical rotational heterogeneity. Single peaks indicate complete rotational frustration.

Although the dense ASX structure has been found both in simulations and nonthermal experiments [15,16], in a

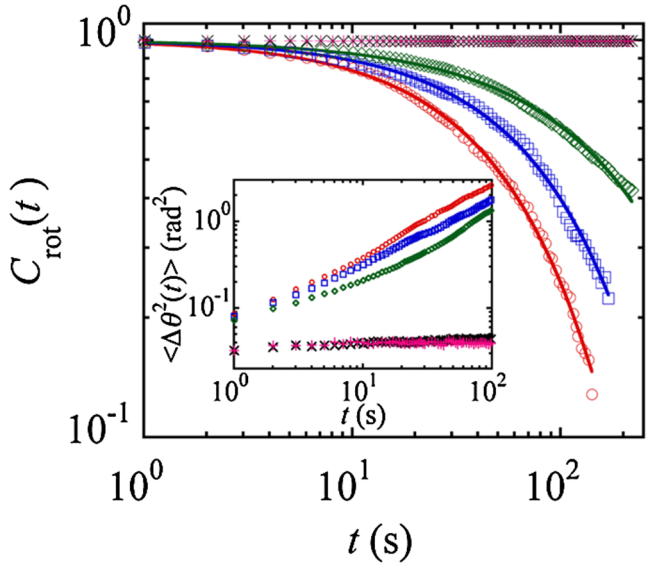

FIG. 4 (color online). Rotational autocorrelation function $C_{\mathrm{rot}}(t)$ at particle area fractions: $\phi_A = 0.66$ (○), 0.70 (□), 0.74 (◇), 0.77 (×), 0.83 (+). Lines: fits to stretched exponential decays with stretching exponents of 0.90 (○), 0.89 (□), and 0.80 (◇). Inset: corresponding mean square angular displacements $\langle \Delta\theta^2(t) \rangle$ for the same ϕ_A.

truly thermal pentagon system, it might be impossible to reach this structure over practical time scales. When compressed from FRX into FRG, pentagons encounter their neighbors even more frequently, and edge-edge configurations are increasingly favored. In the FRG state, tip-tip and tip-edge configurations between neighboring pentagons are not mechanically stable; these configurations can easily destabilize to create defects. These defects eliminate positional QLRO, and the system becomes both rotationally and spatially jammed, precluding access to a possible ASX phase. Even for nonthermal excitations, other observations have revealed several ASX clusters having different orientations (with grain boundaries) [15], not a single crystal.

The observed high-density phases and states for pentagons may also be found for other shapes, including heptagons, that cannot fully tile a flat 2D plane. Although the disorder-order transition is well known, the FRX-FRG transition is peculiar, and the ϕ_A associated with such spatial order-disorder transitions will depend on particle shape. For instance, monodisperse disks would not exhibit either the RX-FRX or the FRX-FRG transitions. We anticipate that Brownian polygons that cannot fully tile a plane will typically display an order-disorder transition in 2D that is a consequence of geometrical frustration. Particles that can fully tile the plane, yet have a different symmetry than hexagonal, might exhibit interesting crystal-crystal or crystal-liquid crystal transitions at high ϕ_A, rather than disorder due to rotational and translational jamming. On a broader level, systems of Brownian polygons could potentially provide direct visual models of frustrated interactions in spin glasses [28] that have either structural order or disorder.

Further exploiting highly anisotropic depletion attractions, which we have shown can be used to create and study 2D monolayers of hard Brownian platelets, will provide experimental 2D phase diagrams and quenched disordered states for particles having a wide range of shapes. We anticipate that these measurements will guide the development of a general picture of shape-dependent phase behavior of Brownian dispersions in 2D.

We thank the National Science Foundation (CHE0450022) for partial support.

*Corresponding author.
mason@physics.ucla.edu

[1] C. A. Murray and D. H. Van Winkle, Phys. Rev. Lett. **58**, 1200 (1987).
[2] A. J. Armstrong, R. C. Mockler, and W. J. O'Sullivan, J. Phys. Condens. Matter **1**, 1707 (1989).
[3] J. R. Savage *et al.*, Science **314**, 795 (2006).
[4] F. Ebert *et al.*, Rev. Sci. Instrum. **80**, 083902 (2009).
[5] K. J. Strandburg, Rev. Mod. Phys. **60**, 161 (1988).
[6] D. R. Nelson, *Defects and Geometry in Condensed Matter* (Cambridge Univesity Press, Cambridge, 2002).
[7] J. A. Cuesta and D. Frenkel, Phys. Rev. A **42**, 2126 (1990).
[8] M. A. Bates and D. Frenkel, J. Chem. Phys. **112**, 10 034 (2000).
[9] Y. Martínez-Ratón, E. Velasco, and L. Mederos, J. Chem. Phys. **122**, 064903 (2005).
[10] A. Donev *et al.*, Phys. Rev. B **73**, 054109 (2006).
[11] K. Zhao *et al.*, Phys. Rev. E **76**, 040401(R) (2007).
[12] E. B. Sirota *et al.*, J. Chem. Phys. **98**, 5809 (1993).
[13] R. P. A. Dullens *et al.*, Phys. Rev. Lett. **96**, 028304 (2006).
[14] C. L. Henley, Phys. Rev. B **34**, 797 (1986).
[15] Y. L. Duparcmeur, A. Gervois, and J. P. Troadec, J. Phys. Condens. Matter **7**, 3421 (1995).
[16] T. Schilling *et al.*, Phys. Rev. E **71**, 036138 (2005).
[17] A. C. Branka and K. W. Wojciechowski, Phys. Lett. A **101**, 349 (1984).
[18] C. J. Hernandez and T. G. Mason, J. Phys. Chem. C **111**, 4477 (2007).
[19] D. Dendukurl *et al.*, Nature Mater. **5**, 365 (2006).
[20] M. Sullivan *et al.*, J. Phys. Condens. Matter **15**, s11 (2003).
[21] J. C. Love *et al.*, Langmuir **17**, 6005 (2001).
[22] A. B. D. Brown, C. G. Smith, and A. R. Rennie, Phys. Rev. E **62**, 951 (2000).
[23] M. D. Hoover *et al.*, J. Aerosol Sci. **21**, 569 (1990).
[24] See EPAPS Document No. E-PRLTAO-103-027948 for the detail of analysis. For more information on EPAPS, see http://www.aip.org/pubservs/epaps.html.
[25] K. Zhao and T. G. Mason, Phys. Rev. Lett. **99**, 268301 (2007); **101**, 148301 (2008).
[26] J. C. Crocker and D. G. Grier, J. Colloid Interface Sci. **179**, 298 (1996).
[27] P. G. Debenedetti and F. H. Stillinger, Nature (London) **410**, 259 (2001).
[28] C. D. Dominicis and I. Giardina, *Random Fields and Spin Glasses* (Cambridge Univ. Press, Cambridge, 2006).